

SIMULATING THE SUNYAEV-ZEL'DOVICH EFFECT(S): INCLUDING RADIATIVE COOLING AND ENERGY INJECTION BY GALACTIC WINDS

MARTIN WHITE¹, LARS HERNQUIST² AND VOLKER SPRINGEL³

¹Departments of Astronomy and Physics, University of California, Berkeley, CA 94720

²Harvard-Smithsonian Center for Astrophysics, Cambridge, MA 02138

³Max-Planck-Institut für Astrophysik, Karl-Schwarzschild-Strasse 1, 85748 Garching, Germany

Draft version November 18, 2018

ABSTRACT

We present results on the thermal and kinetic Sunyaev-Zel'dovich (SZ) effects from a sequence of high resolution hydrodynamic simulations of structure formation, including cooling, feedback and metal injection. These simulations represent a self-consistent thermal model which incorporates ideas from the ‘pre-heating’ scenario while preserving good agreement with the low density IGM at $z \sim 3$ probed by the Ly- α forest. Four simulations were performed, at two different resolutions with and without radiative effects and star formation. The long-wavelength modes in each simulation were the same, so that we can compare the results on an object by object basis. We demonstrate that our simulations are converged to the sub-arcminute level. The effect of the additional physics is to suppress the mean Comptonization parameter by 20% and to suppress the angular power spectrum of fluctuations by just under a factor of two in this model while leaving the source counts and properties relatively unchanged. We quantify how non-Gaussianity in the SZ maps increases the sample variance over the standard result for Gaussian fluctuations. We identify a large scatter in the Y-M relation which will be important in searches for clusters using the SZ effect(s).

Subject headings: cosmic microwave background – cosmology: theory – galaxies: clusters: general – large-scale structure of universe – methods: numerical

1. INTRODUCTION

On angular scales below $10'$, the microwave sky carries the imprint of large-scale structure in the low- z universe. In particular, cosmic microwave background (CMB) photons propagating through the universe are inverse Compton or Doppler scattered by hot electrons along their path, either in dense structures such as clusters of galaxies or more generally in hot gas in the intergalactic medium. Inverse Compton scattering conserves the number of photons but preferentially increases their energy, leading to a spectral distortion whose amplitude is proportional to the product of the electron temperature and density (or pressure). Doppler scattering induces an intensity fluctuation with the same spectral shape as the CMB itself. These effects were first described by Sunyaev & Zel'dovich (1972, 1980) and are known as the thermal and kinetic SZ effects, respectively (for recent reviews see Rephaeli 1995 and Birkinshaw 1999).

The thermal effect is one of the primary sources of secondary anisotropies in the CMB on small angular scales. The change in the (thermodynamic) temperature of the CMB resulting from scattering off non-relativistic electrons is

$$\frac{\Delta T}{T} = y \left(x \frac{e^x + 1}{e^x - 1} - 4 \right) \quad (1)$$

$$\simeq -2y \quad \text{for } x \ll 1, \quad (2)$$

where $x = h\nu/kT_{\text{CMB}} \simeq \nu/56.85$ GHz is the dimensionless frequency, and the second expression is valid in the Rayleigh-Jeans limit which we shall assume henceforth. The quantity y is known as the Comptonization param-

eter and is given by

$$y \equiv \sigma_T \int d\ell \frac{n_e k(T_e - T_{\text{CMB}})}{m_e c^2}, \quad (3)$$

where the integral is performed along the photon path. Since $T_e \gg T_{\text{CMB}}$ the integrand is proportional to the integrated electron pressure along the line of sight.

The kinetic SZ effect arises from the motion of ionized gas with respect to the rest-frame of the CMB. The resulting temperature fluctuation is $\Delta T/T = -b$, where

$$b \equiv \sigma_T \int d\ell n_e \frac{v_r}{c} \quad (4)$$

measures the magnitude of the effect along the line of sight if v_r is the radial peculiar velocity of the gas (positive if the cluster is moving away from us, negative if it is moving towards us). The different dependence on frequency of the two effects can, in principle, be used to disentangle them observationally, though the primary CMB anisotropies provide ‘noise’ for the kinetic SZ signal.

In this paper, we report results of a sequence of high resolution hydrodynamic simulations designed to study the SZ signal on small angular scales. The imprint of the SZ effects on the CMB has been studied by a number of authors (Ostriker & Vishniac 1986; Persi et al. 1995; da Silva et al. 2000, 2001; Refregier et al. 2000; Seljak et al. 2000; Kay, Liddle & Thomas 2001; Refregier & Teyssier 2001; da Silva et al. 2001; Zhang, Pen & Wang 2002). Ours are the first such simulations to incorporate the effects of radiation and star formation, including gas cooling and feedback from supernovae and galactic winds. As such they extend our earlier work on the subject, reported in Springel, White & Hernquist (2001).

arXiv:astro-ph/0205437v2 8 Jul 2002

The outline of this paper is as follows. In Section 2, we briefly describe our simulations and the techniques we use to compute SZ maps. In Section 3, we present our results for the power spectra of thermal and kinetic SZ effects and discuss the effects of non-Gaussianity on the sample variance. We show SZ source counts as a function of source strength and source size and how SZ source properties correlate with the intrinsic properties of the cluster. Finally, we summarize and discuss our results in Section 4.

2. METHOD

We chose as our cosmological model the currently favored Λ CDM cosmology. In particular, we adopted $\Omega_m = 0.3$, $\Omega_\Lambda = 0.7$, $H_0 = 100 h \text{ km s}^{-1} \text{ Mpc}^{-1}$ with $h = 0.7$, $\Omega_B = 0.04$, $n = 1$ and $\sigma_8 = 0.9$. This model yields a reasonable fit to the current suite of cosmological constraints and as such provides a good framework for making realistic predictions. The simulation domain was a $100 h^{-1} \text{ Mpc}$ cube with periodic boundary conditions. We ran smoothed particle hydrodynamic (SPH) simulations at two different mass resolutions corresponding to 2×144^3 and 2×216^3 particles, with initial conditions constructed such that the large-scale modes were equal for both resolutions, allowing us to perform a resolution study on an object by object basis without being affected by cosmic variance. For each mass resolution, we performed a simulation that computed only adiabatic¹ gas physics and shock heating, and one that also followed the radiative cooling and heating processes of the gas in the presence of a UV background radiation field together with star formation and feedback processes in the dense collapsed gas. In Table 1, we list some basic numerical parameters of the four simulations that we carried out.

Radiative cooling and heating was modeled as in Katz, Weinberg & Hernquist (1996), with a photo-ionizing flux similar to the one advocated by Haardt & Madau (1996). Radiation from quasars reionizes the Universe at redshift $z \simeq 6$ in this scenario (for details, see e.g. Davé, Hernquist, Katz & Weinberg 1999). We have treated star formation in the framework of an effective multi-phase model for the interstellar medium (ISM), as detailed by Springel & Hernquist (2002a). In this model, rapidly cooling gas of high overdensity is assumed to give rise to the formation of cold clouds, embedded in an ambient hot medium. The cloud material forms the reservoir of baryons available for star formation. Massive stars are taken to explode as supernovae on a short timescale, and to release their energy as heat to the ambient medium of the ISM. Supernovae are also assumed to evaporate cold clouds, thereby establishing a tight self-regulation cycle for the star-forming ISM.

In addition, we have included a phenomenological model for galactic outflows in our simulations, motivated by the large body of observational evidence for the ubiquitous existence of such galactic winds (e.g. Martin 1999). Galactic-scale outflows are thought to play a crucial role in the enrichment of the low-density intergalactic medium with heavy elements and for the global regulation of star formation, and they may have influenced the properties of intragroup and intracluster gas in a decisive way. Note

¹In what follows, we will refer to the runs that ignored radiative effects and star formation as ‘adiabatic’ but it should be kept in mind that these simulations did include shock heating and so are not strictly speaking adiabatic.

that without the inclusion of such strong feedback processes, simulations tend to substantially overpredict the luminosity density of the universe (Balogh et al. 2001). However, the model for galactic winds that we use here is able to reduce the global efficiency of cooling and star formation sufficiently to match these constraints (Springel & Hernquist 2002c).

In this model, each star-forming galaxy drives a wind with a mass-outflow rate equal to two times its star formation rate, and with a wind-velocity of $v_w = 484 \text{ km s}^{-1}$. These choices are deliberately ‘extreme’ in the sense that the total kinetic energy of the wind is of the order of the energy released by the supernovae. However, these parameters are quite typical for the observed properties of outflows from star-forming disks. Whether or not the wind can escape from a galaxy depends primarily on the depth of its dark matter potential well. Halos with virial temperatures below $\sim 10^6 \text{ K}$ can lose some of their baryons to an outflowing wind, while more massive halos will contain the wind, such that the wind becomes progressively more unimportant for the regulation of star formation in more massive objects.

The simulations considered here are part of a larger simulation program which shows that the particular feedback model we employ allows a numerically converged prediction for the total star formation density of the universe as a function of epoch, provided all star-forming halos above virial temperatures of 10^4 K can be resolved. Of course, the simulations analyzed here cannot reach such a high mass resolution, because they need to model a volume large enough to contain rich clusters of galaxies. It is thus inevitable that part of the star formation is lost due to resolution limitations. This can be a sizable effect. Springel & Hernquist (2002c) show that about 50% of all stars are born in halos with virial masses below $10^{12} h^{-1} M_\odot$, which corresponds roughly to the mass of the smallest halos in our G4 simulation with reliable estimates for the star formation rate. Note that the ‘unresolved’ star formation in

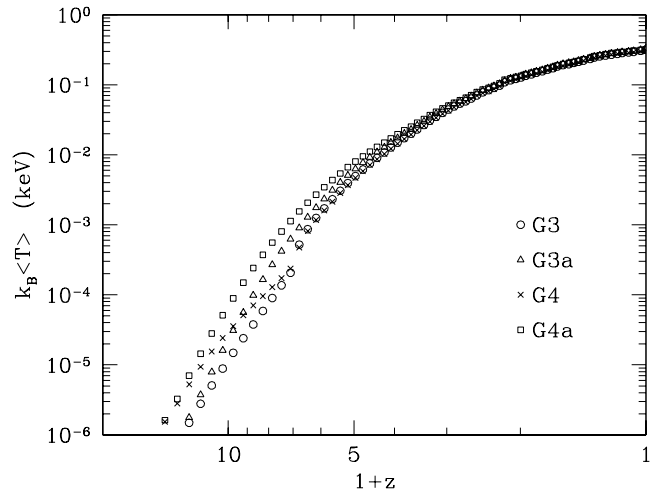


FIG. 1.— The evolution of the mean (mass weighted) temperature in the 4 simulations. Parameters for the simulations can be found in Table 1, an ‘a’ after the name indicates that feedback and cooling were not included.

small halos is also the one that would predominantly be able to drive truly outflowing winds. It should therefore be kept in mind that the effects of galactic outflows on the intracluster medium are likely going to be underestimated by the present simulations.

The simulations were performed on an Athlon-MP cluster at the Center for Parallel Astrophysical Computing (CPAC) at the Harvard-Smithsonian Center for Astrophysics. We used a modified version of the GADGET-code (Springel, Yoshida & White 2001), and integrated the entropy as the independent thermodynamic variable (Springel & Hernquist 2002b).

In all our runs, the full simulation box was output every $100 h^{-1}\text{Mpc}$ along the line-of-sight between redshifts $z \simeq 19$ and $z = 0$. This corresponds to 77 dumps per model. We made maps² in a manner similar to da Silva et al. (2000) as described in our earlier paper (Springel et al. 2001). To recap briefly we stacked the various outputs from the boxes back along the line of sight, with each box randomly translated and oriented in the direction of either the x , y or z axis. Then, a grid of 512^2 rays subtending a constant angle of 1° from the observer was traced through the boxes starting at $z = 19$.

We produced maps of the y -parameter, the Doppler b -parameter, the projected gas density and the thermal bremsstrahlung emission. In the adiabatic simulations we do not track the ionization fraction, x_e , dynamically. Instead, we set it to 1.158, corresponding to full ionization, for temperatures above 10^4K and take the gas at lower temperature to be neutral. The extra physics models self-consistently track x_e and this is used in the computation.

It is also convenient to have a ‘cluster catalog’ from the simulations. We produced this by running a friends-of-friends group finder (e.g. Davis et al. 1985) with a linking length of $b = 0.15$ (in units of the mean inter-particle spacing). The FoF algorithm partitions the particles into equivalence classes by linking together all particle pairs separated by less than a distance b . We define the center of each halo as the position of the potential minimum, calculating the potential using only the particles in the FoF group. This proved to be more robust than using the center of mass, as the potential minimum coincided closely with the density maximum for all but the most disturbed clusters. Additionally, the position of the center was very insensitive to the presence or absence of the particles near

²The missing factor of h in our code which caused the maps from Springel et al. (2001) to be in error has been corrected here.

Model	N_p	M_{DM}	M_{gas}	ϵ
G3	2×144^3	2.5	0.4	18
G4	2×216^3	0.7	0.1	12

TABLE 1

THE PARAMETERS OF THE SIMULATIONS RUN. THE SIMULATION BOX WAS $100 h^{-1}\text{MPC}$ ON A SIDE. PARTICLE MASSES ARE GIVEN IN UNITS OF $10^{10} h^{-1} M_\odot$. GRAVITY WAS SOFTENED WITH A SPLINE ON A COMOVING SCALE ϵ (IN $h^{-1}\text{kpc}$), WITH THE FORCE BEING FULLY NEWTONIAN BEYOND 2.8ϵ AND THE POTENTIAL OF A SINGLE PARTICLE BEING $-Gm/\epsilon$ AT ZERO LAG, EQUIVALENT TO A PLUMMER-SOFTENING ON THE SAME SCALE.

the outskirts of the halo, and thus to the precise linking length used. For each of the halos we computed the mass, M_{200} , enclosed within a radius, r_{200} , interior to which the density contrast was 200 times the critical density. We shall sometimes refer to this as the virial radius, and denote its angular extent at the distance of the cluster by θ_{200} .

3. RESULTS

The evolution of the mean (mass weighted) temperature in the simulations is shown in Fig. 1. The formation of structure in the universe leads to a steady heating with the mean temperature today being approximately $1/3\text{keV}$. We can see the effects of cooling most clearly at early times in the suppression of $\langle T \rangle$ in runs G3 and G4 with respect to G3a and G4a, but by $z = 0$ most of the differences have disappeared. The slight jump in $\langle T \rangle$ at $z \sim 6$ is due to reionization by quasars in this model, which raises the background radiation field and leads to increased photo-heating of the gas in the universe.

We show a typical example of our thermal SZ maps in Fig. 2. These maps were produced by coadding a large number of partial maps, each giving the contribution of one of the boxes that we stacked along the photons’ path. We made 15 maps for each of the 4 simulations, using the same set of random offsets and orientations for each of the 4 simulations. As we noted before (Springel et al. 2001) filaments, while prominent in the partial maps, are largely hidden in the high level of background arising from the

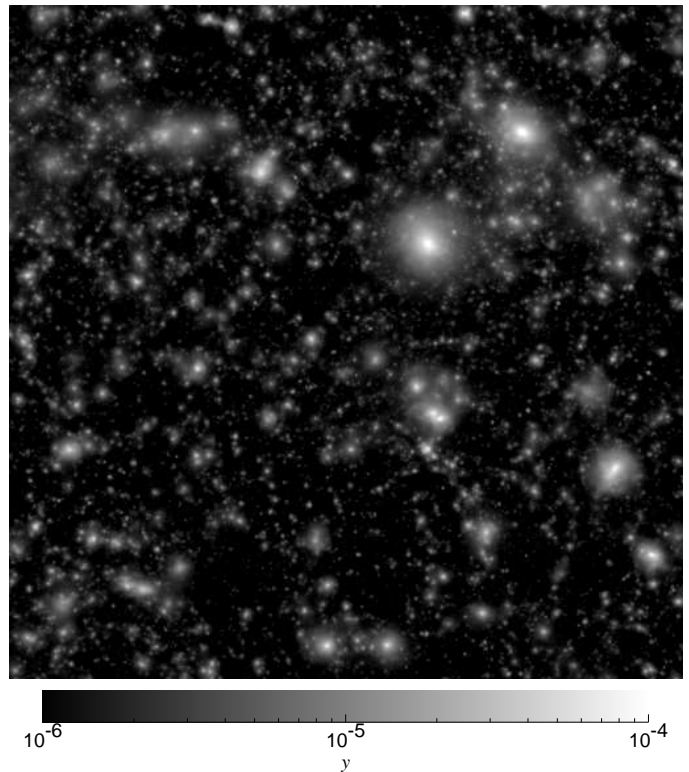


FIG. 2.— One of our Compton y maps, from the simulation G4 including cooling and feedback as described in the text. The corresponding map from the adiabatic simulation looks almost identical to the eye.

summation over many of these structures (see also Croft et al. 2001).

The mean Comptonization we predict from our 15 maps is 2.4×10^{-6} and 2.5×10^{-6} for the lower and higher resolution adiabatic models respectively. This becomes 2.2×10^{-6} and 2.1×10^{-6} for the runs with cooling and feedback. Thus we see that the effect of cooling is more important than heating in aggregate for the gas contributing to the mean y distortion and that our models easily pass the constraint from FIRAS (Fixsen et al. 1996).

3.1. Power spectra

For each map we computed a number of statistics, and we in general averaged the results for 15 random lines of sight to reduce field-to-field variance. Here we present the angular power spectrum of the thermal and kinetic SZ effects (Fig. 3).

A comparison of the low and high resolution simulations indicates that for the adiabatic case we have converged in the angular power spectrum out to $\ell \sim 20,000$. These results are also in excellent agreement with our earlier estimates (Springel, White & Hernquist 2001) once we take into account the slight differences in the cosmological model. For the runs including cooling we are more sensitive to the effects of finite mass and spatial resolution. The higher resolution simulation shows a lower power spectrum than the lower resolution spectrum, indicating that cooling has been able to proceed more efficiently when the simulation can correctly resolve denser structures. However, the final results are quite insensitive to extra physics included in these models, as might have been expected if the bulk of the signal is coming from gas outside the core of the cluster, and the gas content of the intracluster medium is not significantly depleted by gas cooling. In this respect our results differ from those of da Silva et al. (2001) who found a significant effect on the SZ signal if they include cooling in their simulations. The addition of star formation and energy injection in our simulations stabilizes the runaway cooling which otherwise occurs and significantly reduces the impact of the extra physics on the SZ effect. In the absence of such feedback the cooling is only mitigated by numerical resolution, leading to an excess of cold gas and stars in conflict with observations.

The power spectra we predict are in accord with recent measurements of arcminute angular scale anisotropy in the CMB at BIMA (Dawson et al. 2001; 2002) though lower than the detection quoted by CBI (Mason et al. 2002; Bond et al. 2002) from their deep field (the data from mosaic observations, Pearson et al. 2002, do not significantly constrain the signal at high- ℓ). To bring the adiabatic model into agreement with the CBI points would require us to e.g. increase σ_8 to 1–1.2 (or dramatically increase Ω_B ; see e.g. Seljak, Burwell & Pen 2000 or Bond et al. 2002). The inclusion of cooling and feedback lowers our predictions by $\sim 30\%$ on CBI scales, which could be compensated for by an additional $\sim 4\%$ change in σ_8 .

We have also estimated the amount by which the evident non-Gaussian nature of the SZ signal increases the field-to-field variance in the power spectrum. For a Gaussian signal the fractional error per mode in the power spectrum is $\sqrt{2}$, so we expect the standard deviation in the binned power to be $\sqrt{2/N} C_\ell$ where N is the number of modes in the bin. If we compare this expectation to the standard

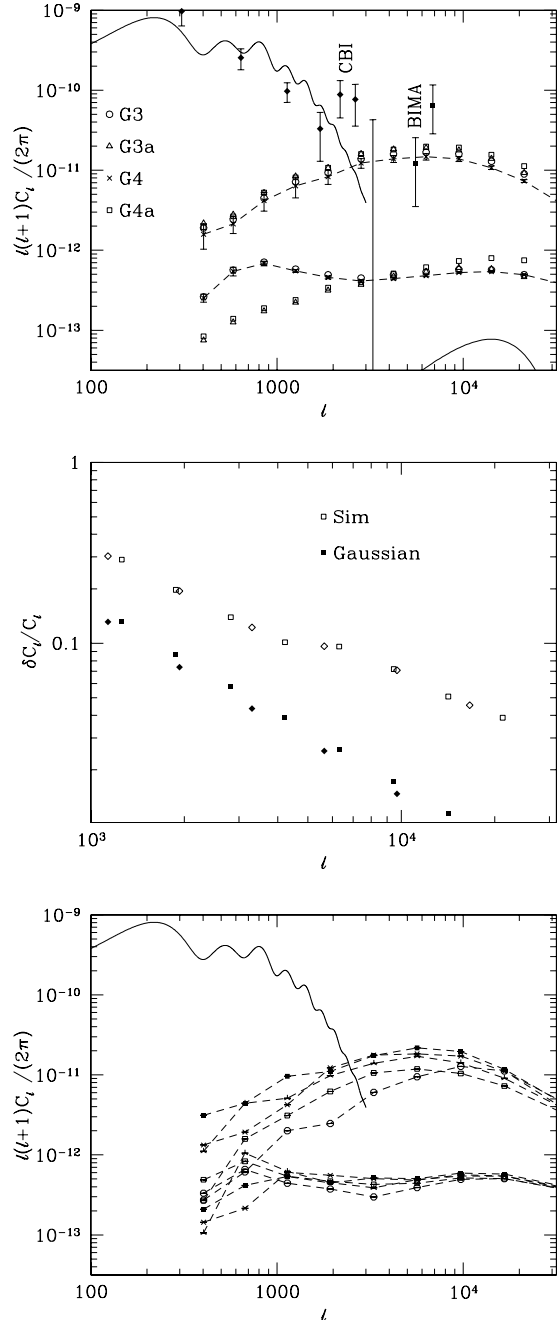


FIG. 3.— (Top) The angular power spectra for the thermal and kinetic SZ effects averaged over 15 maps for each of our 4 simulations. Parameters for the simulations can be found in Table 1, an ‘a’ after the name indicates that feedback and cooling were not included. The upper solid curve shows the primary anisotropy signal for this model (including the effects of lensing). The symbols show the mean SZ signal and the error bars the standard deviation of the power from the 15 maps. A dashed line connects the results of simulation G4. The lower solid curve is an estimate of the effects of patchy reionization assumed to occur at $z = 6$. The points with error bars are observational results from BIMA and CBI (see text). (Middle) The fractional error in the thermal effect, per binned C_ℓ , obtained from the variance of the 15 simulated fields (open symbols) compared to the expectations for a Gaussian sky (filled symbols). Symbol types denote two different binnings of the power spectrum. The non-Gaussian nature of the SZ signal increases the field-to-field scatter over the Gaussian expectation. (Bottom) The angular power spectra for 5 of our fields, showing that the field-to-field fluctuation is primarily in the amplitude, and not the shape, of the spectra.

deviation computed from the 15 maps (Fig. 3), we find that the latter is higher by a factor of 2 (at $\ell \sim 10^3$) to 5 (at $\ell \sim 10^4$) due to the contributions from the 3- and 4-point functions (e.g. Meiksin & White 1999, §2). Since the non-Gaussianity leads to mode-coupling, the exact ratio depends slightly on the binning chosen – we show two choices. We caution the reader that all of the maps are created from the same underlying simulation volume, and so are not fully independent. This makes the estimates at lower ℓ somewhat uncertain. We do not have enough maps to accurately calculate the off-diagonal elements of the correlation matrix (which converge slowly compared to the diagonal elements), however the correlations are strong. As for the non-linear mass power spectrum, the primary fluctuation from field to field is in the amplitude, and not the shape, of the power spectrum. We show an example from 5 of our fields in Fig. 3.

Finally it is of interest to ask where the majority of the thermal SZ signal is coming from in the angular power spectrum – i.e. diffuse gas or gas within halos. To answer this we remade two of our maps excluding all gas with density smaller than $100 \bar{\rho}_{\text{gas}}$. Gas in halos should have higher density than this. The resulting maps are indistinguishable by eye, even ‘blinking’ between them. There is a small (25%) suppression of power for $\ell < 2000$ in the maps with the density cut, but the suppression is $< 2\%$ by $\ell = 6000$ where the signal peaks. This suggests (da Silva et al. 2001) that even the large-angle signal is coming primarily from relatively high density gas along the line-of-sight – the virialized halos – and not from the diffuse gas or filamentary structures (the ‘cosmic web’). If we increase the cut even further, to $10^3 \bar{\rho}_{\text{gas}}$, we start to significantly reduce the thermal SZ signal up to $\ell \sim 10^4$, indicating that the dense cores of the halos do not dominate the thermal SZ signal.

3.2. Source counts

A glance at Fig. 2 indicates that the SZ effect is dominated by discrete sources and that the pixel distribution is highly non-Gaussian. Thus a power spectral analysis contains only a small part of the information in the map. To obtain an understanding of the SZ source sizes and strengths we have used the source detection software SExtractor (Bertin & Arnouts 1996) to count individual sources, and to measure their strength. We used default settings for the detection algorithm of the image processing software and let it estimate background and ‘noise’ levels automatically. Note that our maps are in principle noise-free, so what is interpreted as noise in this procedure effectively arises from limitations due to source confusion, which leads to non-detections of some of the faintest and smallest sources. In a typical analysis with SExtractor, we resolve slightly more than half of the total SZ signal into discrete sources.

We measure the strength of a source as the monochromatic brightness change

$$S_\nu = \int_{\Omega} \Delta B_\nu d\Omega = f(x) B_\nu \int_{\Omega} y(\theta) d\Omega \quad (5)$$

of the CMB integrated over the solid angle of the source. Here B_ν is the Planck spectrum of the primary CMB, and

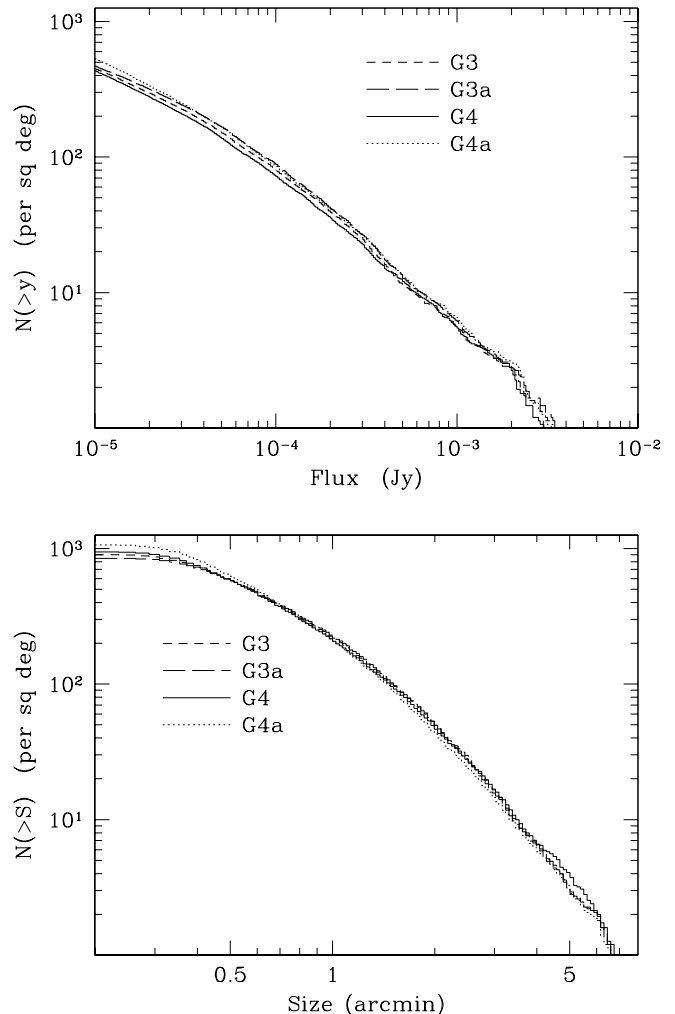


FIG. 4.— Upper panel: the cumulative distribution of source fluxes at $\nu = 30\text{GHz}$. Lower panel: the cumulative distribution of source sizes.

$f(x)$ is the spectral function

$$f(x) = x \frac{e^x}{e^x - 1} \left(x \frac{e^x + 1}{e^x - 1} - 4 \right), \quad (6)$$

with $x = h\nu/kT_{\text{CMB}}$ and we have taken $\nu = 30\text{GHz}$.

In Fig. 4, we show the cumulative source counts per square degree found in the simulations. Again we find remarkably good agreement between all of the simulations, with the cooling runs predicting fewer sources at the bright end by 20-30% and at the faint end by 30-50% (at fixed flux). This is not terribly surprising at the bright end where the source counts are more massive clusters. In this case the bulk of the ICM is at too low a density to cool efficiently. However our calculations suggest that this holds true even for the relatively weak SZ sources. Cooling and feedback thus appear to be a small effect on the clustering and number counts of sources, with the gas dominating the SZ signal being more prone to cooling than heating in our model.

Each of these bright sources is associated with at least one massive halo in the simulation. It is instructive to pursue this association further. In Fig. 5 we show a scatterplot of source strength vs. halo mass, both intrinsic and from the maps. For the ‘intrinsic’ effect we calculated the SZ signal coming from the most massive clusters in our box at $z = 0$. Specifically we summed the SZ signal within half of r_{200} to obtain the total decrement intrinsic to the cluster:

$$Y_{\text{int}} = (\gamma - 1)(1 - Y_p)\sigma_T \sum_j \mu_j x_j \frac{m_j u_j}{m_e c^2} \quad (7)$$

where $\gamma = 5/3$, $Y_p = 24\%$, σ_T is the Thomson cross section, m_e the electron mass, c the speed of light, μ_j is the mean molecular weight of particle j , x_j is the fractional ionization (relative to hydrogen), m_j is the mass and u_j the internal energy. The sum is over all particles within $r_{200}/2$ of the potential minimum in the group, which is the region dominating the SZ emission. Since y is dimensionless we quote Y_{int} in units of $(h^{-1}\text{Mpc})^2$. As the total signal scales as $M \times T$ and for self-similar clusters $T \sim M^{2/3}$ we expect $Y_{\text{int}} \sim M^{5/3}$ which is a good fit to our simulations. The upper panel of Fig. 5 shows that there is a very tight relation between Y_{int} and M_{200} , as has been noted before by e.g. Holder et al. (2000). It is this relation which is behind the claims that a y -selected sample will be close to mass limited.

However, Y_{int} is not an observable. To mimic something which is closer to what an observation could probe we first found all of the clusters in the simulation which fell in the line-of-sight of a particular map. For each of these we integrated the Compton y parameter values in pixels which lay within half θ_{200} of the cluster center to obtain $Y_{\text{map}} = \int d\Omega y$. As the lower panel of Fig. 5 shows, there is a large amount of scatter in this $Y_{\text{map}} - M$ relation, even for our noise free, high resolution maps. This scatter is approximately constant as we vary the aperture used to define Y_{map} and can be traced to 3 prime sources. First, there is evolution in the $M - T$ relation with redshift, and the clusters we have plotted are from a range

³The degree of correlation is almost independent of the exact aperture used.

of redshifts. Second, clusters are not spherical, leading to differences in signal when viewed from different orientations. Finally, the signal we see is the projection of SZ signal from the entire line-of-sight⁴. Since the signal is not dimmed by distance, objects all along the line-of-sight can contribute a significant amount to the signal in any pixel. A similar ‘confusion’ effect operates for optical and weak lensing cluster searches (White & Kochanek 2002; White, van Waerbeke & Mackey 2002). Since clusters form in high density regions, with a lot of dense material nearby, there is a non-negligible chance that some lines of sight will be enhanced by non-cluster material. The extreme outliers in Fig. 5 are all clusters closer to the observer than about $600 h^{-1}\text{Mpc}$, whose virial radii subtend a large angle and are most likely to suffer from this projection effect. These clusters are marked with crosses in the figure.

To isolate this effect further we have computed the integrated SZ signal coming from spheres of gas, centered on rich clusters, viewed from many random directions. Specifically, we first extract all of the gas particles in the simulation within a distance r_{cut} of the minimum of the cluster potential. From this set we compute, using Eq. (7), the total Y for all particles whose 2D projected radius $R < r_{200}/2$ for several lines-of-sight. We also compute Y

⁴This contribution was not included in the work of Holder et al. (2000) who simulated only gas within the virial regions of their sources.

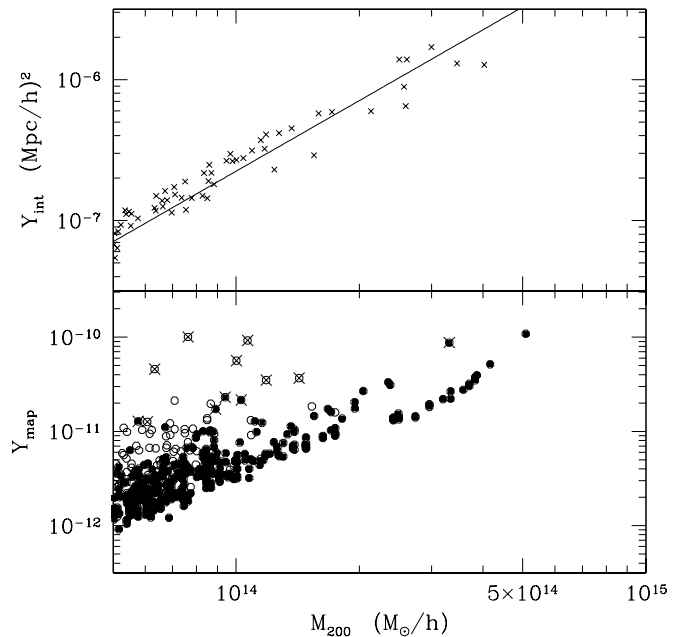


FIG. 5.— The relation between the total decrement, Y , and cluster mass M_{200} . The upper panel shows the decrement calculated from the material within half the virial radius r_{200} for each cluster in the simulation volume at $z = 0$. The straight line indicates $Y_{\text{int}} \propto M_{200}^{5/3}$. The lower panel indicates the decrement obtained directly from the noise free maps by summing pixels centered on the known locations of clusters (excluding clusters near the edge of the map). Open circles indicate clusters whose disk overlapped that of a more massive cluster in the map. Filled circles are ‘isolated’ clusters. Crosses indicate clusters within $600 h^{-1}\text{Mpc}$ of the observer. The source of the scatter is discussed in the text.

from the subset of the particles contained within our FoF group.

Our results are shown in Fig. 6 for $r_{\text{cut}} = 5 h^{-1} \text{Mpc}$ and $r_{\text{cut}} = 10 h^{-1} \text{Mpc}$. For several clusters there is a large scatter between lines-of-sight depending on the presence or absence of material near the cluster. The scatter is larger for the larger radius, indicating that it is not just neighboring material which drives the scatter. If we include only those particles within the FoF group we still see a large scatter, though the SZ signal is noticeably depressed. Thus, some of the scatter is coming from asphericity of the cluster, but a non-negligible fraction of the signal is coming from non-cluster material along some lines-of-sight.

The large scatter that we see in the SZ signal at fixed mass has implications for SZ searches for galaxy clusters – any method which uses primarily SZ flux in target selection will not be mass limited. In fact, the steeply falling mass functions predicted by hierarchical theories would imply that some high-flux candidates are likely to be low mass groups with abnormally high SZ signal rather than the intrinsically rarer rich clusters. If this is true, a blind SZ search should turn up many groups in addition to the desired cluster sample.

4. CONCLUSIONS

We have performed a sequence of high resolution hydrodynamic simulations of structure formation in a ΛCDM model to investigate the effect of extra physics on the thermal and kinetic Sunyaev-Zel'dovich effects. Including only adiabatic gas physics our simulations of the thermal effect are converged down to sub-arcminute scales and agree well with our earlier work. For the runs with extra physics we see an increased efficiency of cooling in the higher resolution simulation which leads to a lowering of the mean Compton y parameter and a slight depression in the SZ angular power spectrum. Overall however the effects of

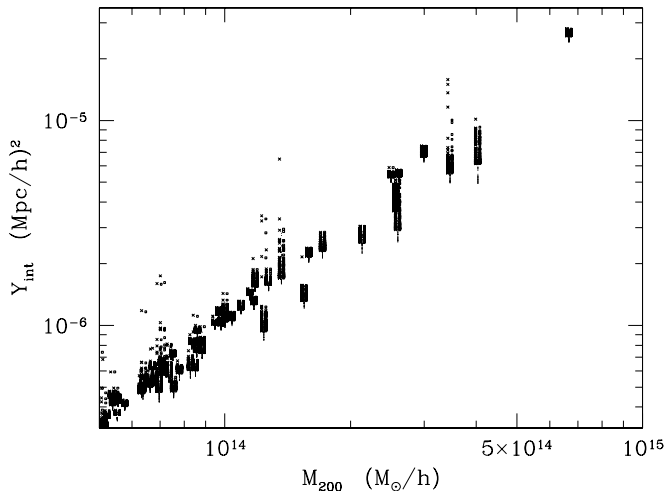


FIG. 6.— The scatter in the $Y_{\text{int}} - M$ relation coming from material close to the clusters. Y_{int} is calculated for each cluster in the simulation volume at $z = 0$ when viewed down 64 random lines of sight. Only material within $R_{200}/2$ in projection was included. Crosses include all material with $r_{\text{cut}} = 10 h^{-1} \text{Mpc}$, open squares $r_{\text{cut}} = 5 h^{-1} \text{Mpc}$ and dots only the material belonging to the FoF group. Points have been offset (horizontally) for clarity.

including the extra physics on the 1- and 2-point functions are slight, indicating that the SZ effect is not overly sensitive to the (uncertain) thermal history of the gas.

The maps are noticeably non-Gaussian and dominated by discrete sources. This non-Gaussianity manifests itself in increased scatter, by a factor of 2-6, in C_ℓ from field-to-field compared to the Gaussian expectation.

The properties of the sources in the map are quite insensitive to the extra physics we have included also, and we are thus able to make robust statements about their detection. The brightest SZ sources have a density of ~ 1 per square degree and their detection requires an angular resolution of $\sim 1'$, and the capability to separate brightness fluctuations of size $\sim 10 \text{mJy}$ from the primary CMB fluctuations.

We have found that there is significant scatter in the SZ fluxes within apertures centered on clusters. This scatter has 3 sources: evolution of the mass temperature relation, asphericity in the matter distribution and line-of-sight projection. The existence of this scatter means that surveys using only SZ flux will select objects with a wide range of masses, including lower mass groups.

We would like to acknowledge useful conversations with Kyle Dawson, Bill Holzapfel, Adrian Lee and Saul Perlmutter. This work was supported by ACI 96-19019, AST 98-02568, AST 99-00877, AST 00-71019. M.W. was supported by a NASA Astrophysical Theory Grant and a Sloan Fellowship. The simulations were performed at the Center for Parallel Astrophysical Computing at the Harvard-Smithsonian Center for Astrophysics.

REFERENCES

- Balogh, M. L., Pearce, F. R., Bower, R. G., & Kay, S. T. 2001, MNRAS, 326, 1228
 Bertin E., Arnouts S., 1996, A&AS, 117, 393
 Birkinshaw M., 1999, Phys. Rep., 310, 98
 Bond J.R., et al., 2002, preprint [astro-ph/0205386]
 Croft, R.A.C., Di Matteo, T., Davé, R., Hernquist, L., Katz, N., Fardal, M. & Weinberg, D.H. 2001, ApJ, 557, 67
 Davé, R., Hernquist, L., Katz, N., & Weinberg, D. H. 1999, ApJ, 511, 521
 Davis M., Efstathiou G., Frenk C.S., White S.D.M., 1985, ApJ, 292, 371
 Dawson K.S., Holzapfel W.L., Carlstrom J.E., Joy M., LaRoque S.J., Reese E.D., 2001, ApJ, 553, L1
 Dawson K.S., et al., 2002, preprint [astro-ph/0206012]
 Fixsen D.J., Cheng E.S., Gales J.M., Mather J.C., Shafer R.A., Wright E.L., 1996, ApJ, 473, 576
 Haardt, F. & Madau, P. 1996, ApJ, 461, 20
 Holder, G.P., Mohr, J.J., Carlstrom, J.E., Evrard, A.E., Leitch, E.M., 2000, ApJ, 544, 629
 Katz, N., Weinberg, D. H., & Hernquist, L. 1996, ApJS, 105, 19
 Kay S.T., Liddle A.R., Thomas P.A., 2001, preprint [astro-ph/0102352]
 Martin, C. L. 1999, ApJ, 513, 156
 Meiksin A., White M., 1999, MNRAS, 308, 1179
 Ostriker J.P., Vishniac E.T., 1986, ApJ, 306, L51
 Mason B.S., et al., 2002, preprint [astro-ph/0205384]
 Pearson T.J., et al., 2002, preprint [astro-ph/0205388]
 Persi F., Spergel D.N., Cen R., Ostriker J.P., 1995, ApJ, 442, 1
 Refregier A., Komatsu E., Spergel D.N., Pen U.-L., 2000, Phys. Rev. D, 61, 123001
 Refregier A., Teyssier R., 2001, preprint [astro-ph/0012086]
 Rephaeli Y., 1995, ARA&A, 33, 541
 Seljak U., Burwell J., Pen U.-L., 2000, preprint [astro-ph/0001120]
 da Silva A.C., Barbosa D., Liddle A.R., Thomas P.A., 2000, MNRAS, 317, 37
 da Silva A.C., Barbosa D., Liddle A.R., Thomas P.A., 2001, MNRAS, 326, 155
 da Silva A.C., Kay S.T., Liddle A.R., Thomas P.A., Pearce F.R., Barbosa D., 2001, ApJ, 561, 15

- Springel, V. & Hernquist, L. 2002a, to appear in: Proceedings of the IAU Symposium 208, edited by J. Makino and P. Hut
- , 2002b, MNRAS, 333, 649, astro-ph/0111016
- , 2002c, in preparation.
- Springel V., Yoshida N., White S.D.M., 2001, NewA, 6, 79 [astro-ph/0003162]
- Springel V., White M., Hernquist L., 2001, ApJ, 549, 681 [erratum: ibid, 562, 1086]
- Sunyaev R.A., Zel'dovich Ya. B., 1972, Comm. Astrophys. Space Phys., 4, 173
- Sunyaev R.A., Zel'dovich Ya. B., 1980, ARA&A, 18, 537
- White M., Kochanek C., 2002, ApJ, in press [astro-ph/0110307]
- White M., van Waerbeke L., Mackey J., 2002, ApJ, in press [astro-ph/0111490]
- Zhang P., Pen U.-L., Wang B., 2002, preprint [astro-ph/0201375]